Backward diodes using heavily Mg-doped GaN growth by ammonia molecular-beam epitaxy

Hironori Okumura, Denis Martin, Marco Malinverni, and Nicolas Grandjean

Citation: Applied Physics Letters **108**, 072102 (2016); doi: 10.1063/1.4942369
View online: http://dx.doi.org/10.1063/1.4942369
View Table of Contents: http://scitation.aip.org/content/aip/journal/apl/108/7?ver=pdfcov
Published by the AIP Publishing

Backward diodes using heavily Mg-doped GaN growth by ammonia molecular-beam epitaxy

Hironori Okumura,[1,2,a)] Denis Martin,[2] Marco Malinverni,[2] and Nicolas Grandjean[2]
[1]*Institute of Applied Physics, University of Tsukuba, 305-8573 Ibaraki, Japan*
[2]*Institute of Condensed Matter Physics, École Polytechnique Férérale de Lausanne (EPFL), CH-1015 Lausanne, Switzerland*

(Received 7 December 2015; accepted 5 February 2016; published online 18 February 2016)

We grew heavily Mg-doped GaN using ammonia molecular-beam epitaxy. The use of low growth temperature (740 °C) allows decreasing the incorporation of donor-like defects ($<3\times10^{17}\,\mathrm{cm}^{-3}$) responsible for *p*-type doping compensation. As a result, a net acceptor concentration of $7\times10^{19}\,\mathrm{cm}^{-3}$ was achieved, and the hole concentration measured by Hall effect was as high as $2\times10^{19}\,\mathrm{cm}^{-3}$ at room temperature. Using such a high Mg doping level, we fabricated GaN backward diodes without polarization-assisted tunneling. The backward diodes exhibited a tunneling-current density of 225 A/cm^2 at a reverse bias of −1 V at room temperature. © *2016 AIP Publishing LLC*. [http://dx.doi.org/10.1063/1.4942369]

Interband tunneling has attracted a lot of interests in semiconductor physics and is a key component for various device applications thanks to the unique characteristics of negative differential resistance (NDR)[1] and electrical connection in series of *p-n* junctions of disparate bandgap.[2] For III-nitride semiconductors, interband tunneling is useful to further improve the performance of optical devices, i.e., light-emitting diodes (LEDs),[3,4] vertical cavity-surface emitting lasers (VCSELs),[5,6] and multi-junction solar cells.[7] In principle, interband tunneling requires ultra-thin *p-n* junction depletion width (w_d) and therefore degenerates semiconductors. III-nitride compounds have suffered from a low tunneling probability (T_t) due to the difficulty to get degenerate impurity doping and high potential-barrier heights (Ψ_{bi}). Recently, GaN-based tunnel junctions (TJs) were achieved using polarization-assisted tunneling.[8] Those TJs exhibit current-voltage (*I-V*) characteristics with a backward-diode behavior, which shows a tunneling current at small reverse bias. GaN/AlN/GaN[8] and GaN/InGaN/GaN heterostructures[9] were proposed to take advantage of the high internal electric fields that builds up from the interfacial polarization-induced dipoles along the *c*-axis and which allows reducing w_d. However, an InGaN interlayer requires precise control of both the thickness and the indium compositions, and it could induce detrimental absorption losses in VCSELs. On the other hand, TJ devices with an AlN interlayer are hampered by a low reverse current density (<10 A/cm^2 at −5 V) due to the wide bandgap of AlN (6.05 eV). The realization of GaN TJs without polarization-assisted tunneling is thus of prime interest to take advantage of the full potential of GaN-based optical devices.

In ideal *p-n* junctions, w_d is given by $(2\varepsilon_s\Psi_{bi}/q\,(N_A+N_D/N_AN_D))^{1/2}$, where ε_s, N_A, and N_D are the permittivity (=9.8ε_0 for GaN using permittivity (ε_0) in vacuum),[10] the acceptor concentration, and the donor concentration, respectively. The relationship between N_A and w_d in GaN *p-n* junction with $N_D=1\times10^{20}\,\mathrm{cm}^{-3}$ is shown in Fig. 1. As expected, w_d decreases with increasing doping concentration but even for high N_A values ($>5\times10^{19}\,\mathrm{cm}^{-3}$) it remains below 10 nm without polarization-assisted tunneling. Under the Wentzel–Kramers–Brillouin approximation, T_t is given by[11]

$$T_t \cong \exp\left(-2\int_0^{w_d}\sqrt{\frac{2m_t^*E_g\mathrm{x}}{\hbar^2 w_d}}\,\mathrm{dx}\right). \quad (1)$$

Here, m_t^* is the tunneling effective mass, E_g is the bandgap of semiconductors, and $\hbar$ is the reduced Planck's constant. Assuming that for GaN TJs with polarization-assisted tunneling w_d equals the interlayer thickness, then T_t for GaN/2.8-nm-thick AlN/GaN[8] and GaN/6-nm-thick $In_{0.3}Ga_{0.7}N$/GaN[9] structures is estimated to be $\sim10^{-12}$ and $\sim10^{-18}$, respectively. On the other hand, T_t of GaN TJs without polarization-assisted tunneling is much lower, typically 10^{-33} for $N_A=5\times10^{19}\,\mathrm{cm}^{-3}$. The dependence of T_t on N_A in GaN TJs without polarization-assisted tunneling is displayed in Fig. 1. From Eq. (1), we note that a high T_t requires small bandgap and/or thin w_d. In GaN-based optical devices,

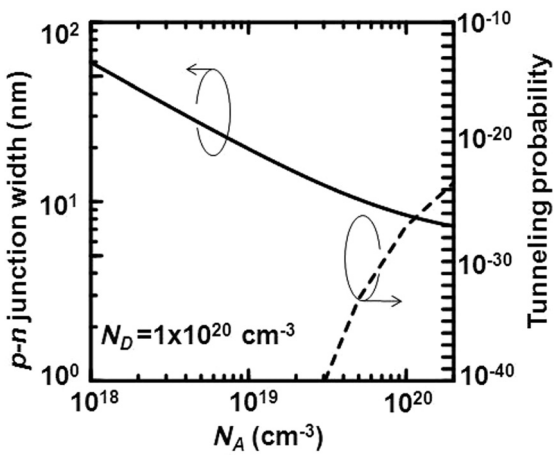

FIG. 1. Depletion width and tunneling probability of a GaN *p-n* junction calculated as a function of N_A for $N_D=1\times10^{20}\,\mathrm{cm}^{-3}$ using Equation (1).

a)Electronic mail: okumura.hironori.gm@u.tsukuba.ac.jp

TJs should be reversely biased thereby reducing w_d and significantly increasing T_t ($>10^{-20}$ at -1 V). Nevertheless, superior backward-diode behavior does require thin w_d and therefore heavily doped GaN.

p-type GaN epilayers can be grown by molecular-beam epitaxy (MBE) or by metal-organic vapor phase epitaxy (MOVPE). In both growth techniques, the conventional *p*-type dopant is magnesium, which acts as an acceptor by substituting for Ga sites. In Mg-doped GaN (GaN:Mg), the ionized acceptor concentration (N_A^-) is intrinsically low due to the high ionization energy (E_a) of Mg ($\sim$185 meV),[12] and because of compensation induced by inversion-domain boundaries and pyramidal defects in heavily Mg-doped GaN[13] and donor-like defects such as nitrogen vacancy (V_N).[14] In addition, a post-growth process, e.g., a rapid thermal annealing (RTA), is required for *p*-type GaN grown by MOVPE to activate Mg acceptors from Mg-H complexes.[15] On the other hand, MBE growth of *p*-type GaN does not need RTA post-growth processes and the formation of compensation defects is hindered due to low growth temperature ($\sim$750 °C).[16] In this study, we report on the electrical properties of heavily Mg-doped GaN grown using ammonia MBE and on the demonstration of GaN backward diodes without polarization-assisted tunneling.

For all GaN growth, we used 4-μm-thick GaN (0001) templates grown on 2-in. c-plane sapphire substrates by MOVPE. Before growth, molybdenum was deposited on the substrate backside using sputtering for heat coupling. GaN templates cleaved into half were loaded into the MBE chamber, followed by baking out at 500 °C for 1 h in ultra-high vacuum to remove any residual surface contamination. The MBE chamber is equipped with effusion cells for Ga evaporation and purified ammonia gas to deliver the nitrogen species by on-surface cracking. We use N-rich growth regime, i.e., a high ammonia flow (>50 sccm) owing to the low thermal decomposition efficiency ($\sim$4%) of ammonia.[17] After a 1-μm-thick unintentionally doped (UID) GaN buffer growth, a 0.5 μm-thick *p*-type GaN layer was deposited using an ammonia flow rate of 120 sccm (background pressure of 1.2×10^{-5} Torr in main chamber) and a Ga beam equivalent pressure (BEP) of 3.4×10^{-7} Torr. The growth rate was 5.5 ± 0.2 nm/min. Mg *p*-type dopant was supplied by a Riber VCOR 110 valved cell at 250 °C and silicon *n*-type dopant by a conventional effusion cell. The Mg-doping concentration [Mg] was controlled by valve opening (BEP between 0.9 and $4.2\times10-^{10}$ Torr). For GaN:Mg growth, low growth temperature (<700 °C) induces surface roughening due to Ehrlich–Schwoebel barrier at step edges on the surface.[18] On the other hand, higher growth temperature (>750 °C) leads to high compensation ratio of Mg acceptors, as defined by $([Mg]-(N_A-N_D))/[Mg]>20\%$.[16,19] In this study, the GaN:Mg layers were grown at a temperature of 740 °C.

The growth temperature and growth thickness of GaN were monitored using an optical pyrometer and spectral reflectance, respectively. During GaN growth, the reflection high-energy electron diffraction (RHEED) patterns were streaky, indicating two-dimensional (2D) growth mode. Impurity concentrations of GaN:Mg were determined by secondary ion mass spectrometry (SIMS) performed by Evans Analytical Group. Detection limits for hydrogen, carbon, oxygen, Si, and Mg are 2×10^{18}, 3×10^{16}, 2×10^{16}, 4×10^{16}, and 4×10^{16} cm^{-3}, respectively. The net acceptor concentration (N_A–N_D) and hole concentration (p) in the GaN:Mg layers were determined by electrochemical capacitance-voltage (*C-V*) measurements and by Hall effect measurements at room temperature, respectively. The ohmic contacts for the *C-V* and Hall-effect measurements were obtained by metal indium paste and Pd (50 nm)/Au (200 nm) metal stack without RTA processes, respectively.

N_A–N_D as a function of Mg flux for 500-nm-thick GaN:Mg layers is shown in Fig. 2(a). N_A–N_D linearly increases with Mg fluxes, suggesting efficient incorporation of Mg atoms into the GaN layers. We could control the lower limit of N_A-N_D to 3×10^{17} cm^{-3}, indicating that the GaN:Mg layer has a fairly low concentration of compensation defects ($<10^{17}$ cm^{-3}). Notice that the concentration of oxygen and Si in GaN:Mg layers are under the detection limits. Actually, N_A–N_D agrees well with [Mg] measured by SIMS until a critical value of N_A–$N_D=7\times10^{19}$ cm^{-3}. The N_A–N_D of 7×10^{19} cm^{-3} is among the highest values reported so far for *p*-type GaN.[12,20–22] In ammonia MBE, the main donor-like native defects are supposed to be neutral Mg_{Ga}-V_N complex,[23] whose density increases with growth temperature. We speculate that the high N_A–N_D value of

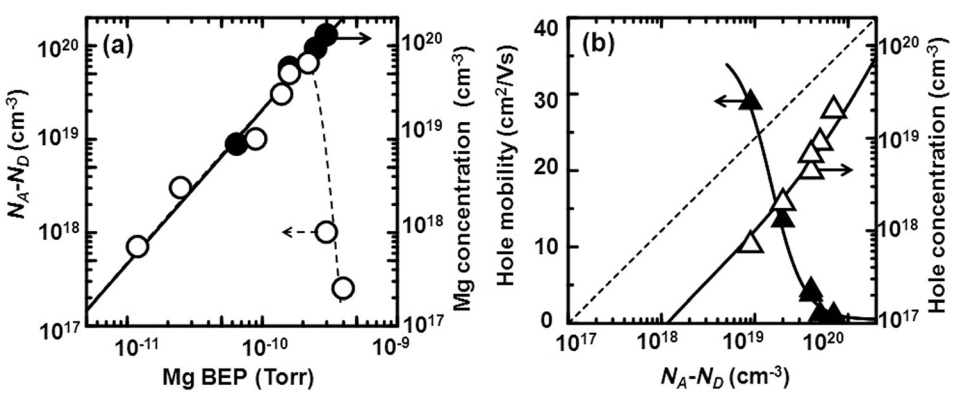

FIG. 2. (a) Relationship between Mg flux and total acceptor concentration (N_A-N_D) determined by capacitance-voltage measurements (white circle), and Mg flux as a function of Mg concentration determined by SIMS (black circle). (b) Room-temperature dependence of Hall concentration (white triangle) and Hall mobility (black triangle) on N_A-N_D for 500-nm-thick GaN:Mg layers. The line for Hall concentration represents the fit of the free hole concentration using Equation (2). The line for Hall mobility is a fit using $\mu_{min}+(\mu_{min}-\mu_{min})/(1+(N_A-N_D/N_{ref})^{\beta})$,[24] where $\mu_{min}=1.0$ cm^2/V s, $\mu_{min}=36$ cm^2/V s, $N_{ref}=1.5\times10^{19}$ cm^{-3}, and $\beta=2.5$.

$7 \times 10^{19}\,\mathrm{cm}^{-3}$ results from a reduction of these compensation defects by precisely controlling the growth conditions, i.e., a careful control of the growth temperature (740 °C), a large NH_3 flow rate (200 sccm), and an optimized growth rate of 5.5 nm/min. By further increasing the Mg flux, N_A–N_D dramatically decreases, in agreement with previous works.[16,22] Further investigations are necessary to clarify the behavior of excess Mg atoms in MBE grown *p*-type layers.

The relationship between hole mobility and N_A–N_D below the critical concentration in 500-nm-thick GaN:Mg layers is displayed in Fig. 2(b). The hole mobility decreases with increasing N_A–N_D, as expected from ionized-impurity scattering. For GaN:Mg layer with N_A–$N_D = 2 \times 10^{19}\,\mathrm{cm}^{-3}$, the room-temperature resistivity, hole mobility, and hole concentration are 0.2 Ω cm, $13.5\,\mathrm{cm}^2/\mathrm{V\ s}$, and $2 \times 10^{18}\,\mathrm{cm}^{-3}$, respectively. A hole concentration of $2 \times 10^{19}\,\mathrm{cm}^{-3}$ is measured for GaN:Mg layers with the highest N_A–N_D value ($=7 \times 10^{19}\,\mathrm{cm}^{-3}$). This increase of the ionization efficiency for high [Mg] is due to a lower E_a.

E_a of Mg acceptors can be estimated from the charge-neutrality conditions in a non-degenerate *p*-type semiconductor[25] and is given by

$$\frac{p + N_D}{N_A - N_D - p} = \frac{N_V}{g} \exp\left(-\frac{E_a}{k_B T}\right), \tag{2}$$

where N_v is the effective density of states in the valence band ($2(2\pi m_h^* k_B T)^{3/2}/h^3$)), g is the acceptor degeneracy (4 for GaN), k_B is the Boltzmann constant, T is the temperature (300 K), and m_h^* is the effective hole mass ($1.25m_0$ for GaN).[26] E_a can be reduced in proportion to the average distance between ionized acceptors ($\sim(N_A^-)^{1/3}$) due to binding energy reduction from Coulomb interaction with ionized acceptors and screening of the Coulomb potential by mobile charges.[27,28] We calculated a reduction of E_a from the Coulomb potential between ionized Mg acceptors and free holes using the equation of $E_a = E_{a0} + fq^2(4\pi/3 \cdot N_A^-)^{1/3}/(4\pi\varepsilon_s)$, where E_{a0} is the acceptor ionization energy in the absence of ionized acceptors, q is the hole charge, and f is a geometric factor. The latter value for various semiconductors is almost constant (-1.6 ± 0.1)[29] and should be mainly dominated by the attractive potential between mobile charges and fixed ions (-1.5).[27] The experimental data were fitted under the assumption of $N_D = 1 \times 10^{17}\,\mathrm{cm}^{-3}$ and $N_A^- \approx p$, as shown in Fig. 2(b). We used $f = -1.69$ and $E_{a0} = 195$ meV, close to the value (188 meV) estimated from the hydrogen-like impurity model ($E_{a0} = 13.6\varepsilon_0^2 m_h^*/(\varepsilon_s^2 m_0)$). For GaN:Mg layers with a maximum N_A–N_D of $7 \times 10^{19}\,\mathrm{cm}^{-3}$, E_a is as small as 29 meV. We conclude that the high hole concentration in GaN:Mg results from a high incorporation of Mg atoms and a screening of the binding energy of Mg acceptors.

Subsequently, we fabricated heavily doped *n-p* junction diodes. The band diagram of the *n-p* junction is shown in Fig. 3(a). We used a structure with thin n^{++} and p^{++} type GaN layers located at the *n-p* interface to get rid of the detrimental effect of surface roughening and crystalline-quality degradation, which occurs in thicker layers. The structure of the *n-p* junction devices consists of the following from the top: 50-nm-thick Si-doped GaN ($N_D \sim 1 \times 10^{20}\,\mathrm{cm}^{-3}$)/15-nm-thick

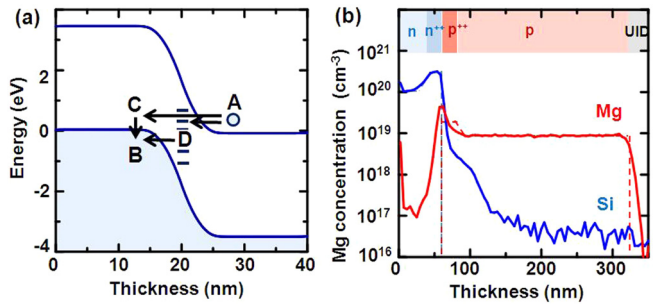

FIG. 3. (a) Energy band diagram of a heavily doped GaN *n-p* junction ($N_A = N_D = 1 \times 10^{20}\,\mathrm{cm}^{-3}$) at zero bias. For reverse and zero biases, carriers are tunneling in the depletion layer through path AB. At forward bias, some carriers might tunnel to local energy levels at C (path ACB) and at D (path ADB), causing excess current. (b) SIMS depth profiles of Si and Mg atoms in heavily doped *n-p* junction of GaN. The detection limit of Si and Mg was equal to $4 \times 10^{16}\,\mathrm{cm}^{-3}$ in both cases. The dotted line is expected doping concentration.

Si-doped GaN ($N_D \sim 3 \times 10^{20}\,\mathrm{cm}^{-3}$)/15-nm-thick Mg-doped GaN ($N_A < 5 \times 10^{19}\,\mathrm{cm}^{-3}$)/200-nm-thick Mg-doped GaN ($N_A \sim 1 \times 10^{19}\,\mathrm{cm}^{-3}$)/500-nm-thick UID GaN grown on GaN templates. High doping concentrations in n^{++} and p^{++} GaN layers were achieved by reducing the growth rate to 3 nm/min. We prepared a series of three *n-p* junction structures with different Mg concentrations of 2×10^{19}, 5×10^{19}, and $1 \times 10^{20}\,\mathrm{cm}^{-3}$ in the p^{++} GaN layers without growth interruption at a constant growth temperature of 740 °C. The impurity concentration in the *n-p* junction with Mg concentration of $2 \times 10^{19}\,\mathrm{cm}^{-3}$ was determined by SIMS. Concentrations of hydrogen, carbon, oxygen, Si, and Mg in UID GaN were under the detection limits. As shown in Fig. 3(b), Si and Mg atoms were uniformly incorporated during growth. Both the Mg rise and decay signals had steep slopes of 7 and 6 nm/decade, respectively. The doping profile of Mg atoms at the *n-p* junction interface exhibits a sharp peak, whose value of $5 \times 10^{19}\,\mathrm{cm}^{-3}$ is higher than the expected Mg-doping concentration of $2 \times 10^{19}\,\mathrm{cm}^{-3}$ and seems to slightly extend into the GaN:Si layer. This high Mg concentration is likely resulting from Mg surface segregation. On the other hand, the small tail of Si concentration of $2 \times 10^{18}\,\mathrm{cm}^{-3}$ into p^{++} GaN may result from unintentional Si incorporation due to low growth rate. Al/Au (30/200 nm) stack was deposited for the *n*-type GaN contact using e-beam evaporation, followed by mesa isolation using Cl_2 plasma in inductively coupled-plasma reactive-ion etching, and then evaporation of Pd/Au (30/200 nm) stack for the *p*-type GaN contact. Both *n*- and *p*-type contacts show ohmic characteristics. The typical resistivity of the *n*- (r_n) and *p*-type (r_p) contacts are estimated to be 2×10^{-5} and 2×10^{-3} $\Omega\,\mathrm{cm}^2$, respectively, using transfer length measurement.

Room-temperature *I-V* characteristics of the *n-p* junction devices ($50\,\mu\mathrm{m} \times 50\,\mu\mathrm{m}$) with [Mg] $\sim 2 \times 10^{19}$, $\sim 5 \times 10^{19}$, and $\sim 1 \times 10^{20}\,\mathrm{cm}^{-3}$ for the *p*-type layer are reported in Fig. 4(a). The devices with [Mg] ($\approx N_A$–N_D) $\sim 2 \times 10^{19}$ and $\sim 5 \times 10^{19}\,\mathrm{cm}^{-3}$ exhibit a backward-diode behavior, in which the reverse current is higher than the forward current at low voltage bias. The backward-diode behavior results from tunneling at reverse bias due to heavy *p*- and *n*-type doping levels. The tunneling-current density (J_T) increases with N_A due to thinner w_d. For [Mg] $\sim 5 \times 10^{19}\,\mathrm{cm}^{-3}$, J_T is 225 A/cm^2 at a reverse bias of −1 V. At higher [Mg] ($\sim 1 \times 10^{20}\,\mathrm{cm}^{-3}$, i.e.,

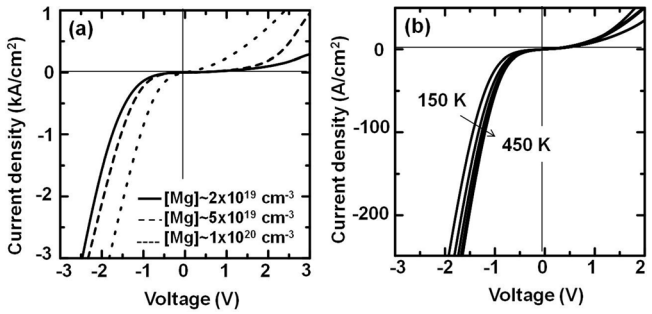

FIG. 4. (a) Current-voltage characteristics of GaN *n-p* diodes ($50 \times 50\,\mu m^2$) for *p*-type layers with [Mg] $\sim 2\times10^{19}, \sim 5\times10^{19}$, and $\sim 1\times10^{20}\,cm^{-3}$ at room temperature. (b) Current-voltage characteristics of GaN *n-p* diodes ($200 \times 200\,\mu m^2$) for [Mg] $\sim 5\times10^{19}\,cm^{-3}$ for temperatures ranging between 150 and 450 K.

$N_A - N_D \sim 10^{18}\,cm^{-3}$), both the reverse and forward current densities increase and the backward-diode behavior vanishes. The larger forward current density is attributed to excess current through energy levels within the forbidden bandgap of GaN. As shown in Fig. 3(a), defective *p*-type GaN layers (point C) and Mg surface accumulation induced defects at the *p-n* interface (point D) may form energy levels in the *p*-type layer and at the *n-p* junction interface, respectively, resulting in high carrier tunneling via ACB and ADB paths. Thus, the higher crystalline quality of *p*-type GaN would further improve the rectifying behavior of the backward diodes. The specific resistivity of the tunnel junction (r_{tj}) is estimated to be $2 \times 10^{-3}\ \Omega\ cm^2$ using the total resistivity ($r_t = r_{tj} + r_n + r_p$) obtained from the linear region of the reverse bias characteristics. Although r_{tj} is comparable with values reported in other reports,[9,16] r_{tj} is close to r_p. A reduction in r_p would thus further enhance J_T.

Temperature dependent *I-V* curves of the *n-p* junction devices ($200\,\mu m \times 200\,\mu m$) with $N_A \sim 5 \times 10^{19}\,cm^{-3}$ are displayed in Fig. 4(b). At forward bias, the rectifying behavior is maintained over a large temperature range (150–450 K). A prominent metric for backward diodes is the curvature coefficient at zero voltage bias, defined as $\gamma = (\partial^2 I/\partial V^2)/(\partial I/\partial V)$.[11] Here γ is $13\,V^{-1}$, which is lower than the thermal limit value $\gamma \sim q/kT \sim 39\,V^{-1}$ for the Schottky barrier. This may be ascribed to high *n*- and *p*-type doping concentrations. Notice that γ is constant ($14 \pm 1\,V^{-1}$) over temperature variation up to 450 K due to the wide bandgap of GaN, like SiC backward diodes.[30] On the other hand, at reverse bias, J_T reduces with decreasing temperature due to larger energy bandgap. One should point out that signature of NDR is not observed even at low temperature. We suppose that thinner w_d using narrower bandgap interlayer and polarization-assisted tunneling is necessary for getting NDR and high J_T. Nevertheless, the J_T obtained in this work is $\sim 1\,kA/cm^2$, which is sufficiently high for applications in LEDs and solar cells. For instance, adding a TJ on top of an LED allows substituting the *p*-GaN layer by a transparent *n*-type GaN layer with much lower contact resistivity.[5]

In conclusion, we grew heavily Mg-doped GaN using ammonia MBE and demonstrated GaN backward diodes without polarization-assisted tunneling. N-rich growth regime at a low growth temperature of 740 °C allows for low concentration of compensation defects ($<3 \times 10^{17}\,cm^{-3}$). Under these growth conditions, we achieved a high net acceptor concentration of $7 \times 10^{19}\,cm^{-3}$ and a high hole concentration of $2 \times 10^{19}\,cm^{-3}$ at room temperature while keeping high hole mobility. The corresponding resistivity is as low as 0.2 Ω cm. Using such a high Mg doping level, we fabricated GaN backward diodes with a rectifying behavior over a large temperature range of 150–450 K. A tunneling-current density of $225\,A/cm^2$ at a reverse bias of -1 V at room temperature is measured, which is suitable for LED applications.

This work was supported by the CTI Project 10708.1 PFNM-NM and JSPS KAKENHI Grant No. 15H06070. We would like to acknowledge Dr. Raphaël Butté for critical reading of the manuscript.

[1]L. Esaki, Phys. Rev. **109**, 603 (1958).
[2]A. Seabaugh and Q. Zhang, Proc. IEEE **98**, 2095 (2010).
[3]S. Jeon, Y. Song, H. Jang, G. Yang, S. W. Hwang, and S. J. Son, Appl. Phys. Lett. **78**, 3265 (2001).
[4]I. Ozden, E. Makarona, A. Nurmikko, T. Takeuchi, and M. Krames, Appl. Phys. Lett. **79**, 2532 (2001).
[5]M. Malinverni, D. Martin, and N. Grandjean, Appl. Phys. Lett. **107**, 051107 (2015).
[6]J. T. Leonard, E. C. Young, B. P. Yonkee, D. A. Cohen, T. Margalith, S. P. DenBaars, J. S. Speck, and S. Nakamura, Appl. Phys. Lett. **107**, 091105 (2015).
[7]A. Luque and A. Marti, Phys. Rev. Lett. **78**, 5014 (1997).
[8]J. Simon, Z. Zhang, K. Goodman, H. Xing, T. Kosel, P. Fay, and D. Jena, Phys. Rev. Lett. **103**, 026801 (2009).
[9]S. Krishnamoorthy, D. N. Nath, F. Akyol, P. S. Park, M. Esposto, and S. Rajan, Appl. Phys. Lett. **97**, 203502 (2010).
[10]H. Morkoc, *Nitride Semiconductor Devices* (Wiley-VCH, 2012), Chap. 1.
[11]S. M. Sze, *Physics of Semiconductor Devices*, 3rd ed. (Wiley, New York, 1981), Chap. 8.
[12]E. C. Kyle, S. W. Kaun, E. C. Young, and J. S. Speck, Appl. Phys. Lett. **106**, 222103 (2015).
[13]P. Vennéguès, M. Benaissa, S. Dalmasso, M. Leroux, E. Feltin, P. D. Mierry, B. Beaumont, B. Damilano, N. Grandjean, and P. Gibart, Mater. Sci. Eng., B **93**, 224 (2002).
[14]C. G. Van de Walle and J. Neugebauer, J. Appl. Phys. **95**, 3851 (2004).
[15]S. Nakamura, N. Iwasa, M. Senoh, and T. Mukai, Jpn. J. Appl. Phys., Part 1 **31**, 1258 (1992).
[16]M. Malinverni, J. M. Lamy, D. Martin, E. Feltin, J. Dorsaz, A. Castiglia, M. Rossetti, M. Duelk, C. Velez, and N. Grandjean, Appl. Phys. Lett. **105**, 241103 (2014).
[17]M. Mesrine, N. Grandjean, and J. Massies, Appl. Phys. Lett. **72**, 350 (1998).
[18]A. L. Corrion, F. Wu, and J. S. Speck, J. Appl. Phys. **112**, 054903 (2012).
[19]A. Dussaigne, B. Damilano, J. Brault, J. Massies, E. Feltin, and N. Grandjean, J. Appl. Phys. **103**, 013110 (2008).
[20]L. Sugiura, M. Suzuki, and J. Nishino, Appl. Phys. Lett. **72**, 1748 (1998).
[21]D. Iida, K. Tamura, M. Iwaya, S. Kamiyama, H. Amano, and I. Akasaki, J. Cryst. Growth **312**, 3131 (2010).
[22]A. Castiglia, J. F. Carlin, and N. Grandjean, Appl. Phys. Lett. **98**, 213505 (2011).
[23]S. Hautakangas, J. Oila, M. Alatalo, and K. Saarinen, Phys. Rev. Lett. **90**, 137402 (2003).
[24]H. Matsuura, M. Komeda, S. Kagamihara, H. Iwata, R. Ishihara, T. Hatekeyama, T. Watanabe, K. Kojima, T. Shinohe, and K. Arai, J. Appl. Phys. **96**, 2708 (2004).
[25]W. Götz, R. Kern, C. Chen, H. Liu, D. Steigerwald, and R. Flatcher, Mater. Sci. Eng., B **59**, 211 (1999).
[26]B. Santic, Semicond. Sci. Technol. **18**, 219 (2003).
[27]G. L. Pearson and J. Bardeen, Phys. Rev. **75**, 865 (1949).
[28]P. P. Debye and E. M. Conwell, Phys. Rev. **93**, 693 (1954).
[29]B. Podor, Semicond. Sci. Technol. **2**, 177 (1987).
[30]J. D. Hwang, Y. K. Fang, K. H. Chen, and D. N. Yaung, IEEE Electron Device Lett. **16**, 193 (1995).